

ARTICLE

<https://doi.org/10.1038/s42003-019-0508-1>

OPEN

Targeting of lipid metabolism with a metabolic inhibitor cocktail eradicates peritoneal metastases in ovarian cancer cells

Rain R. Chen^{1,2}, Mingo M.H. Yung^{1,2}, Yang Xuan¹, Shijie Zhan¹, Leanne L. Leung^{1,2}, Rachel R. Liang^{1,2}, Thomas H.Y. Leung², Huijuan Yang³, Dakang Xu⁴, Rakesh Sharma⁵, Karen K.L. Chan², Siew-Fei Ngu², Hextan Y.S. Ngan^{1,2} & David W. Chan^{1,2}

Ovarian cancer is an intra-abdominal tumor in which the presence of ascites facilitates metastatic dissemination, and associated with poor prognosis. However, the significance of metabolic alterations in ovarian cancer cells in the ascites microenvironment remains unclear. Here we show ovarian cancer cells exhibited increased aggressiveness in ascites microenvironment via reprogramming of lipid metabolism. High lipid metabolic activities are found in ovarian cancer cells when cultured in the ascites microenvironment, indicating a metabolic shift from aerobic glycolysis to β -oxidation and lipogenesis. The reduced AMP-activated protein kinase (AMPK) activity due to the feedback effect of high energy production led to the activation of its downstream signaling, which in turn, enhanced the cancer growth. The combined treatment of low toxic AMPK activators, the transforming growth factor beta-activated kinase 1 (TAK1) and fatty acid synthase (FASN) inhibitors synergistically impair oncogenic augmentation of ovarian cancer. Collectively, targeting lipid metabolism signaling axis impede ovarian cancer peritoneal metastases.

¹The University of Hong Kong Shenzhen Institute of Research and Innovation (HKU-SIRI), Shenzhen, P. R. China. ²Department of Obstetrics & Gynaecology, LKS Faculty of Medicine, The University of Hong Kong, Hong Kong SAR, P. R. China. ³Department of Gynecological Oncology, Fudan University Shanghai Cancer Center, Fudan University, Shanghai 200032, P.R. China. ⁴Faculty of Medical Laboratory Science, Ruijin Hospital, School of Medicine, Shanghai Jiao Tong University, Shanghai 200030, P.R. China. ⁵Proteomics & Metabolomics Core Facility, LKS Faculty of Medicine, The University of Hong Kong, Hong Kong SAR, P. R. China. Correspondence and requests for materials should be addressed to H.Y.S.N. (email: hysngan@hku.hk) or to D.W.C. (email: dwchan@hku.hk)

Ovarian cancer is one of the most common and deadly cancers in women worldwide. The high mortality rate of this cancer is due to its poor prognosis, and most cases are diagnosed at advanced stages accompanied by metastasis generated via transcoelomic spread, which are known as peritoneal metastases or peritoneal carcinomatosis¹. Patients with peritoneal metastases and dissemination to distant sites usually have a poor prognosis. Despite advances in clinical management of this disease^{2,3}, there is still no effective treatment for complete eradication of metastatic ovarian cancer cells, because of the diffuse nature of this cancer as well as the favorable tumor microenvironment in the peritoneal cavity⁴. Approximately 80% of women with ovarian carcinoma present with peritoneal metastases that are often associated with the production of ascites, and of note, most metastatic cancer cells prefer dissemination to adipose tissue-rich environments such as that in the peritoneum and omentum^{5,6}. Accumulating evidence has revealed that malignant ascites and omental microenvironments provide an abundance of soluble growth factors, pro-inflammatory cytokines and fatty acids that are conducive to metastatic ovarian cancer development and invasion^{7,8}. Therefore, understanding the molecular mechanisms associated with effects of the ascites or omental microenvironment on ovarian cancer cell growth and aggressiveness may enable the development of better therapeutic strategies to improve the quality of life of ovarian cancer patients. Recent evidence has shown that omental adipocytes provide fatty acids for rapid tumor growth, and also promote homing, migration, and invasion of ovarian cancer cells^{9,10}. These findings suggest that metastatic ovarian cancer cells may use metabolic reprogramming to utilize lipid metabolism for tumor progression in the fatty acid-enriched microenvironment of the peritoneal cavity. However, the effect of fatty acids on ovarian cancer cell metabolism, and the mechanism by which ovarian cancer cells regulate their metabolism to facilitate tumor dissemination and invasion, remain obscure.

In this study, we report that ovarian cancer cells undergo metabolic reprogramming when cultured in omental conditioned medium (OCM), with lipid metabolism providing energy to ovarian cancer cells through AMPK/ACC signaling. On the other hand, a gradual reduction of AMPK activation due to the subsequent high ATP production led to the activation of mTOR and TAK1/NF- κ B signaling, which in turn, enhanced ovarian cancer metastasis and aggressiveness. Thus, targeting lipid metabolism and/or suppressing TAK1/NF- κ B signaling may be effective therapeutic strategies to prevent and treat peritoneal metastases in ovarian cancer.

Results

OCM enhances ovarian cancer cell oncogenic properties. As the omentum is one of the preferred sites of ovarian cancer cell dissemination, it is of interest to study whether the omental microenvironment provides favorable conditions for ovarian cancer development and metastasis. Consistent with our previous finding¹¹, ovarian cancer cells showed significant increases in cell proliferation when cultured in OCM (Fig. 1a). Similarly, these cancer cells exhibited increased cell migration and invasion rates in OCM (Fig. 1b, c). Using a liquid chromatography tandem-mass spectrometry (LC-MS/MS)-based label-free quantitative proteomics approach and gene ontology analyses, both cellular and metabolic processes are shown to be the most dominant biological functions in OCM-cultured ovarian cancer cells¹² (Fig. 1d). Further analysis using Ingenuity pathway analysis (IPA) on metabolic interaction network revealed that 31 out of 135 upregulated (Fold Change > 1) metabolic targets were associated with lipid metabolism (Fig. 1e–g). These findings suggest that

OCM provides a favorable microenvironment for ovarian cancer development and aggressiveness by increasing cellular and lipid metabolic activities.

OCM provides free fatty acids for ATP production. To determine whether tumor cells utilize free fatty acids from OCM as the energy source to support tumor development and metastasis, we first examined the accumulation of lipid droplets in the cytoplasmic compartment using immunofluorescent and lipid staining analyses. The results suggested that ovarian cancer cells might take up free fatty acids from OCM or ascites, synthesize lipid droplets and store the fatty acids in their cytosol as early as 30 min to 1 h (Fig. 2a) after addition of the medium. Importantly, OCM functioned similarly to ascites such that OCM caused ovarian cancer cells to exhibit an ~0.85- to 2.8-fold increase in lipid droplets (Fig. 2a). Of note, luminescence assays for ATP showed that cellular levels of ATP in ovarian cancer cells were higher by up to 35% when cultured in OCM (Fig. 2b). SKOV3 and ES-2 cells showed an increase in ATP levels up to 7 h and then a decline up to 10 h, whereas OVCA433 and A2780cp cells showed continuous increases in ATP up to 10 h (Fig. 2b). These differences may be due to the different rates of ATP production in different cell contexts, different cell proliferation rates and/or different types of feedback loop controlling ATP production¹³. We found that ES-2 and OVCA433 cells commenced lipolysis and reached the maximal rate at 2 h of culture in OCM, which was followed by a reduction in lipolysis (Fig. 2c). Consistently, AMPK acts as a key energy sensor that maintains cellular energy homeostasis by controlling a number of physiological processes¹⁴. Western blot analysis revealed that the phosphorylation of AMPK at Thr172 became obviously elevated within the first 2–6 h, which was similar to the pattern of lipolysis (Fig. 2c) (Supplementary Fig. 1a) in ovarian cancer cells cultured in OCM. But ovarian cancer cells were cultured for a longer time (> 3 h), the intensity of phospho-AMPK^{Thr172} gradually decreased to levels close or even lower than the basal levels in ovarian cancer cells (Supplementary Fig. 1a), suggesting the reduction in AMPK phosphorylation was attributed to the negative feedback of high ATP production¹⁵. To determine whether fatty acids in OCM are the primary energy source, fatty acids from OCM was first removed by Cleanascite™ Lipid Removal Reagent (Supplementary Fig. 1b)¹⁶. Then, XTT cell proliferation assays showed that the growth rate of ovarian cancer cells was remarkably reduced in cells cultured in Cleanascite-treated OCM (Fig. 2d). Likewise, co-treatment with Cleanascite and OCM significantly attenuated the increased cell migration and invasion capacities of ES-2 and SKOV3 cells (Fig. 2e, f). These findings suggest that the fatty acid-enriched OCM provides as an energy source for supporting tumor growth and aggressiveness of ovarian cancer cells.

Ovarian cancer cells exert metabolic reprogramming in OCM.

It is generally believed that the most prominent metabolic adaptation employed by cancer cells is enhanced glycolysis, known as the Warburg effect¹⁷. To examine whether ovarian cancer cells undergo metabolic reprogramming when cultured in OCM or fatty acid-enriched medium, we first used STF31, an inhibitor of the glucose transporter GLUT1, to inhibit the use of glycolysis to generate energy for supporting ovarian cancer cell growth. XTT cell proliferation assays showed that co-treatment with STF31 led to an initial decline in cell proliferation of ovarian cancer cells, but that long-term culture could restore the cell proliferation rate despite a slightly lower cell proliferation rate than that of cells cultured in OCM (Fig. 3a). In addition, when OCM was co-treated with Cleanascite, the cell proliferation rate was completely impaired as compared with the control OCM

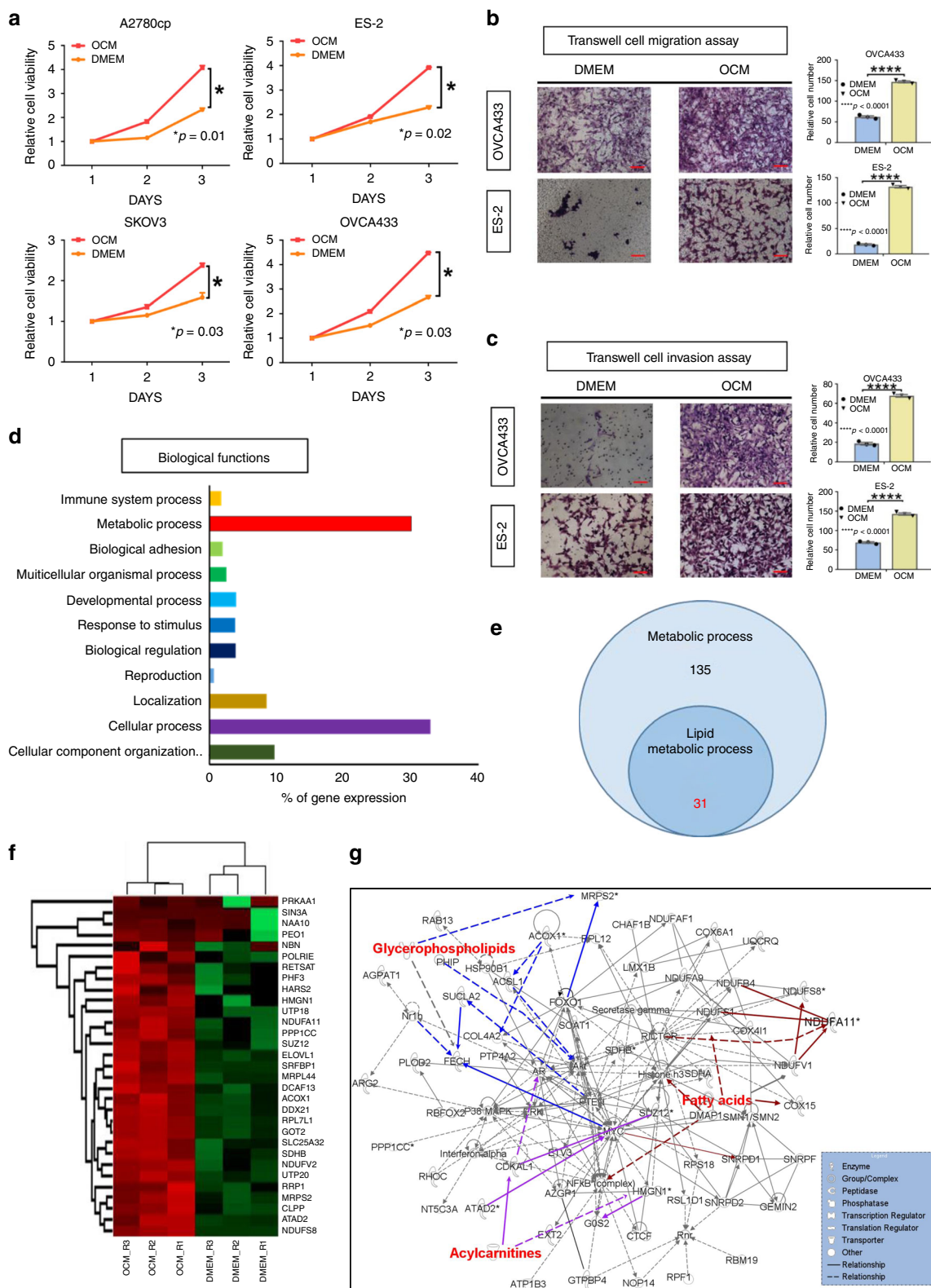


(Fig. 3a). To avoid the concerns of off-target effects of STF31 and Cleanascite, the key glycolytic gene, *SLC2A1* (encoding GLUT1) was stably knocked down using lentiviral shRNAi in OVCA433 and SKOV3 cells. Depletion of GLUT1 did not alter expression of other GLUT isoforms, such as GLUT3 and GLUT4 (Supplementary Fig. 2a). Besides, knockdown of GLUT1 reduced glucose uptake (measured using 2-deoxyglucose) by 65% compared with scrambled control (SC), while the same cells with stably

knockdown of GLUT3 and GLUT4 had no change in glucose uptake capacities (Fig. 3b) (Supplementary Fig. 2a), suggesting that GLUT1 is the primary glucose transporter in ovarian cancer cells.

To confirm the importance of lipolysis and lipogenesis in ATP production, we investigated the role of acetyl-CoA carboxylase (ACC) because it consists of two isoforms: ACC α , which locates in the cytoplasm, is involved in lipogenesis, and ACC β , which

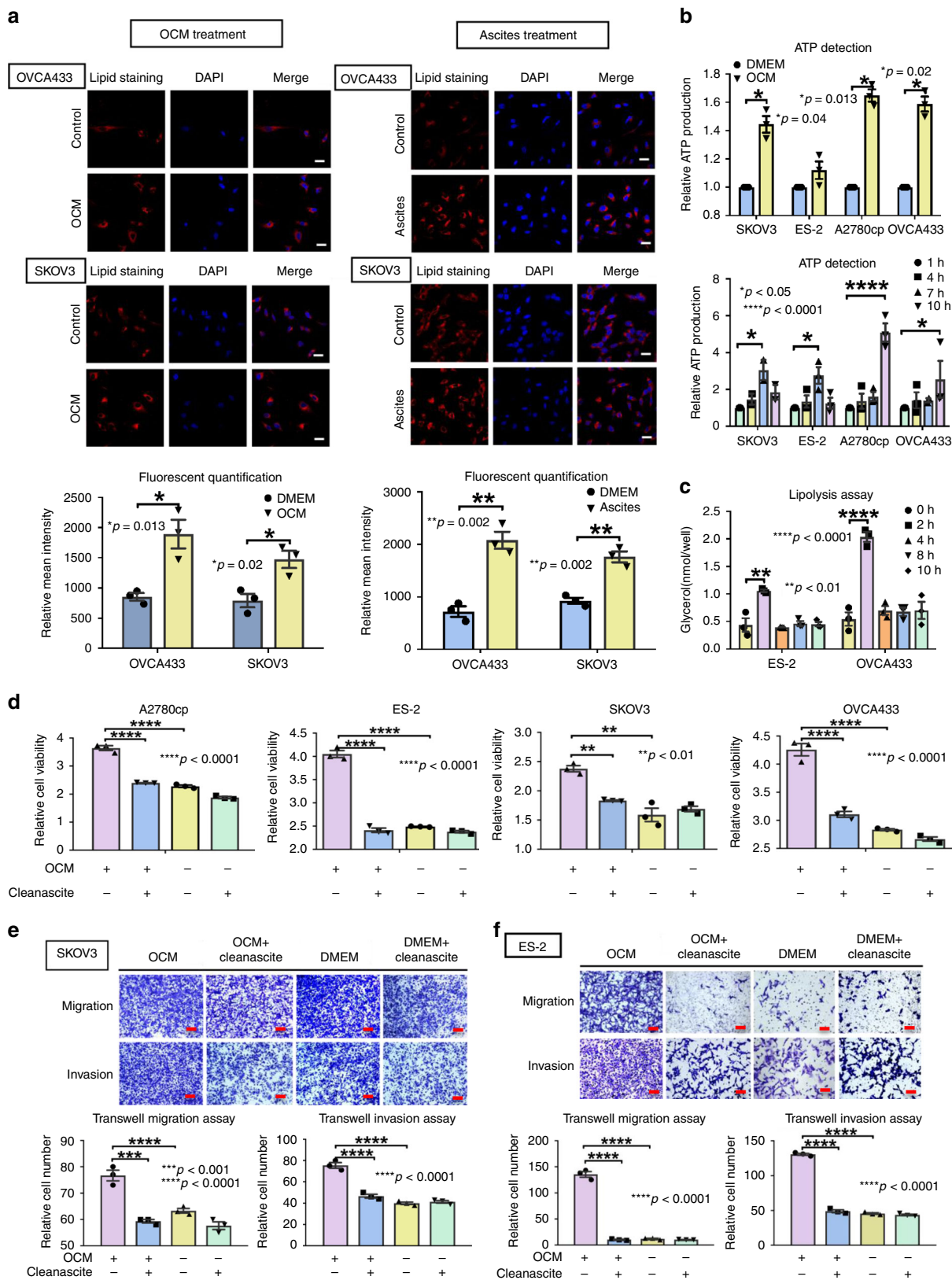
Fig. 1 The lipid metabolic genes are frequently upregulated in ovarian cancer cells when cultured in OCM. **a** XTT cell proliferation assay demonstrates that treatment with OCM significantly increases cell growth in A2780cp, ES-2, SKOV3, and OVCA433 ovarian cancer cells. The relative cell viability was calculated by normalized to the mean value of day 1. **b** Transwell cell migration and **c** transwell cell invasion assays demonstrate that OCM treatment (12–24 h) promotes both cell migratory and invasive capacities in both OVCA433 and ES-2 cells. The stained cells were counted from four selected fields randomly. Representative images and quantitative results of cell migration and invasion were shown. Scale bar = 50 μm . **d** Ontology analysis on the altered genes detected by LC-MS/MS proteomic analysis indicates that most genes altered by OCM are associated with cellular and metabolic processes. The % of gene expression represents the % number of altered genes involved in each category of biological functions vs the total altered genes in ovarian cancer cells cultured in OCM as compared with the DMEM control. **e** A Venn diagram shows 31 out of 135 proteins related to metabolic processes are related to lipid metabolism. **f** Heatmap representation of the expression levels of the 31 proteins related to metabolism. **g** Ingenuity pathway analysis (IPA) depict interaction network of genes related to lipid metabolism in ovarian cancer cells. Results were presented as mean \pm S.E.M. Data were analyzed by Student's *t*-tests, and $*p < 0.05$ was considered as statistical significance

locates at the mitochondrial membrane, controls fatty acid oxidation¹⁸. Using lentiviral shRNAi, both ACC α and ACC β were stably knocked down in SKOV3 and OVCA433 cells (Supplementary Fig. 2b). Interestingly, while depletion of GLUT1 has only a small effect (15–21%) on ATP levels in SKOV3 or OVCA433 cells cultured in OCM, depletion of either ACC α or ACC β resulted in much larger effects (40 to 50%) in both lines (Fig. 3c). This indicates that ACC α and ACC β play more important roles than GLUT1 in lipogenesis (ACC α) and ATP production (ACC β) of ovarian cancer cells cultured in OCM. Functionally, while the XTT cell proliferation assay showed that knockdown of GLUT1 initially influenced cell growth, there was almost no inhibitory effect on cell growth after day 3 or day 4 (Fig. 3d). By contrast, knockdown of ACC α markedly impaired proliferation of both cell lines by 1.6–2-fold (Fig. 3d). Similarly, knockdown of GLUT1 had no effect on lipid droplets, whereas depletion of ACC α obviously reduced the lipid droplet formation in OVCA433 and SKOV3 (Fig. 3e) (Supplementary Fig. 2c). Moreover, knockdown of ACC α obviously inhibited the capacities of cell migration and invasion in ovarian cancer cells, whereas knockdown of GLUT1 had no effect on cell migration/invasion in ovarian cancer cells (Fig. 3f) (Supplementary Fig. 2d). Using an *in vivo* tumor xenograft mouse model, we also demonstrated that knockdown of ACC α reduced 95%, and more than three-fold of tumor weight when compared with SC and knockdown of GLUT1 in SKOV3 cells, respectively (Fig. 3g). Taken together, these results indicate that ovarian cancer cells cultured in OCM or ascites undergo metabolic reprogramming, switching from the use of aerobic glycolysis to the use of lipid metabolism to produce ATP for their tumorigenic capacities.

Ovarian cancer cells undergo lipogenesis in OCM. To better understand how ovarian cancer cells utilized the absorptive fatty acids from OCM, we analyzed the composition of fatty acids in OCM/ascites and ovarian cancer cells by Lipidomic profiling. Results indicated there was a higher accumulation of unsaturated fatty acids (UFA) than saturated fatty acids (SFA) in ovarian cancer cells when cultured in OCM for 24 h (Fig. 4a). Consistently, both OCM and ascites exhibited a higher ratio of UFA to SFA (Supplementary Fig. 3a). Of note, the amount of major UFA oleic acid increased much faster than the SFAs such as stearic acid and palmitic acid decreased from 0 to 24 h in OCM (Fig. 4b), while the amounts of oleic acid, palmitic acid, and linoleic acid were equally distributed in OCM or ascites (Supplementary Fig. 3b). This indicates OCM-cultured ovarian cancer cells has increased activity in biosynthesis of long chain fatty acids for formation of lipid droplets. Fatty acid synthase (FASN) is a key enzyme of biosynthesis of fatty acids^{19,20}, and western blotting clearly showed that the levels of FASN in rapidly growing ovarian cancer cell lines were much higher than the human immortalized normal ovarian epithelial cells (HOSEs) (Fig. 4c), that is consistent with other cancer reports^{19,20}. Depletion of

FASN in ovarian cancer cells by shRNAi caused the reduced content of long chain fatty acids in both OCM and DMEM by twofolds when compared with the scrambled controls (SC) (Fig. 4d, e). Consistently, the depletion of FASN also led to remarkable reduction of lipid droplet formation in ovarian cancer cells (Fig. 4f), supporting the important role of FASN in lipogenesis of ovarian cancer cells²¹. To further confirm that activated FASN and the suppressed phospho-AMPK^{Thr172} due to high ATP production are responsible for enhancing ovarian cancer oncogenic properties in OCM, we added two potent FASN-specific inhibitors (orlistat and GSK2194069 (GSK)) or an AMPK potent activator (PF-06409577 (PF)) to ovarian cancer cells in OCM. These inhibitors completely impaired the increased cell proliferation rate mediated by OCM in ovarian cancer cells (Fig. 4g). Consistently, the depletion of FASN caused a remarkable reduction of cell proliferation, cell migration, and invasion of ovarian cancer cells in OCM (Fig. 4h, i and Supplementary Fig. 4), indicating FASN is another key target for the oncogenic properties of ovarian cancer cells in OCM. Taken together, these findings have suggested that ovarian cancer cells utilize absorbed fatty acids for ATP production and synthesize *de novo* fatty acids used as cellular components to support their increased cell growth in OCM.

Downstream AMPK-regulated oncogenic signaling. Activated AMPK has been shown to impede cell growth and proliferation in part by inhibiting mTORC1 signaling²². In this study, we have shown that AMPK activation was reduced in the presence of OCM due to negative feedback by high ATP content. To determine whether reduced AMPK activity leads to increased oncogenic capacity of ovarian cancer cells, we examined mTORC1 signaling. After 24 h of culture in OCM, the phosphorylation of AMPK at Thr172 was reduced and was inversely correlated with the increased phosphorylation of mTOR at Ser2448 and phospho-pP70S6K Thr389 in ES-2 and SKOV3 ovarian cancer cells after culturing in OCM for 24 h (Fig. 5a). This suggests that the reduced AMPK activity induced activation of mTOR signaling in ovarian cancer cells. However, mTOR signaling could partially explain the enhanced aggressiveness of ovarian cancer cells^{23,24}. We previously reported that increased TAK1 activity, through phosphorylation of Ser412, is required for the activation of the NF- κ B signaling cascade in mediating ovarian cancer metastasis upon treatment with OCM¹¹. Coincidentally, we found that the reduced level of phospho-AMPK^{Thr172} inversely correlated with the increased level of phospho-TAK1^{Ser412} in OVCA433 and ES-2 ovarian cancer cells when cultured in OCM for 24 h (Fig. 5b, c). This result reveals that the reduced AMPK activity favors the activities of TAK1 and NF- κ B in promoting ovarian cancer cell aggressiveness. On the other hand, upon treatment with 6-Chloro-5-[4-(1-hydroxycyclobutyl)phenyl]-1H-indole-3-carboxylic Acid (PF-06409577), a potent and direct AMPK activator²⁵, we



demonstrated that increased AMPK inversely correlated with TAK1 activity of ovarian cancer cells in a dose-dependent manner of PF-06409577 (Fig. 5d). To examine whether TAK1 alters AMPK activity, ovarian cancer cells were co-treated with TAK1 inhibitor 5Z-7-Oxozaenol (5Z-O), and results showed that

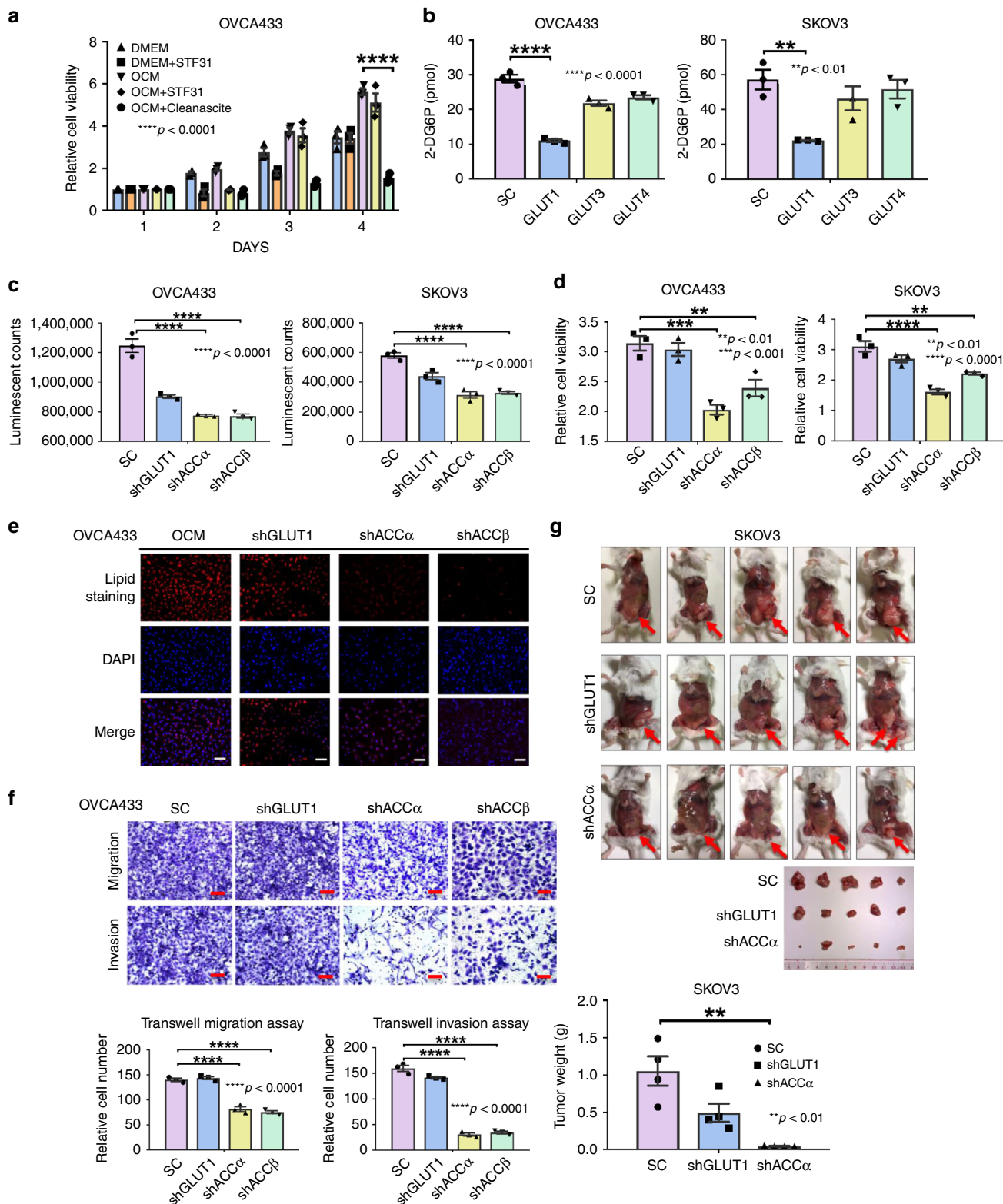
inhibition of TAK1 activity in a dose-dependent manner of 5Z-O slightly enhanced AMPK phosphorylation in SKOV3 only, while there's no effect on AMPK phosphorylation in OVCA433 and SKOV3 cells (Fig. 5e). The slight increase in AMPK activity might be due to the cytotoxicity of 5Z-O in SKOV3 but not in

Fig. 2 Free fatty acids from OCM provide an energy source for ovarian cancer cells. **a** Immunofluorescent and lipid staining analyses demonstrate that ovarian cancer cells SKOV3, OVCA433, A2780cp, and ES-2 exert lipogenesis by free fatty acid uptake from OCM (left panel) or ascites (right panel) and store free fatty acids as lipid droplets (red color by Nile Red staining) in their cytosol. Bar charts show the relative intensity of fluorescent signals (red) of OVCA433 (upper) and SKOV3 (lower) cells cultured in OCM or ascites (freshly obtained from ovarian cancer patients) for 24 h. DMEM (1%) was used as a negative control for both cell lines. Scale bar = 20 μ m. **b** Spectrophotometric analysis and Luminescent ATP Detection Assay show a time-dependent increase in ATP production in SKOV3, ES-2, A2780cp, and OVCA433 cells. Each cell line exhibits the highest ATP production at different time points: SKOV3 and ES-2 for 7 h, while A2780cp and OVCA433 for 10 h. **c** Lipolysis Colorimetric Assay shows lipolysis activity from 0 to 10 h of ES-2 and OVCA433 cells upon culturing in OCM. **d** XTT cell proliferation assay shows that removal of fatty acids from OCM by Cleanascite (1:4 mixed with Cleanascite for 1 h before centrifugation) remarkably reduces the growth of ovarian cancer cells (A2780cp, ES-2, OVCA433, and SKOV3) compared with the negative control Cleanascite treatment in complete DMEM on day 3. Transwell cell migration/invasion assays demonstrate that the removal of free fatty acids by Cleanascite in OCM significantly reduces cell migration and invasion rates in **(e)** SKOV3 and **(f)** ES-2 cells, while the removal of fatty acids by Cleanascite in complete DMEM as negative controls does not change the cell migration or invasion rates of SKOV3 and ES-2 cells. The stained cells for cell migration and invasion were randomly counted from at least four selected fields. The representative images and bar charts were shown. Scale bar = 50 μ m. Results were presented as mean \pm S.E.M. Data were analyzed by Student's *t*-tests or one-way/two-way ANOVA with Tukey's post hoc test ($^*p < 0.05$, $^{**}p < 0.01$, $^{***}p < 0.001$, $^{****}p < 0.0001$)

OVCA433 cells. To address this question, TAK1 in OVCA433 was knocked down by shRNA approach, while there was no change in either phospho-AMPK^{Thr172} or total AMPK levels (Fig. 5f), suggesting AMPK is upstream rather than downstream of TAK1 in ovarian cancer cells. Taken together, the reduced AMPK activity resulting from high ATP content led to activation of both mTORC1 signaling and TAK1/NF- κ B signaling in ovarian cancer cells cultured in OCM.

Targeting AMPK and TAK1 impair ovarian cancer aggressiveness. Given that AMPK acts as an upstream effector of TAK1/NF- κ B signaling, we next investigated whether targeting AMPK alone, or in combination with TAK1 suppression could inhibit the oncogenic capacities of ovarian cancer cells cultured in OCM. Knockdown of AMPK α 1 impaired the activation of AMPK activity in OCM-cultured ovarian cancer cells with different levels due to varied cell context (Fig. 6a). In addition, knockdown of AMPK α 1 favored the growth of ovarian cancer cells in OCM compared with DMEM control (Fig. 6b). However, co-treatment with PF-06409577 could abrogate the increased cell proliferation caused by AMPK α 1 knockdown in ovarian cancer cells in OCM (Fig. 6c). Consistently, co-treatment with TAK1 inhibitor, 5Z-O, in AMPK-knockdown ovarian cancer cells resulted in suppression of cell proliferation, which was similar to the effect of AMPK activator PF-06409577 (Fig. 6c). To better assess the cellular responses to drug treatments, we performed 3D spheroid ovarian cancer cell culture for OVCA433 and ES-2 and co-treated with PF-06409577, Orlistat and 5Z-O alone at serial diluted concentrations or in combination. Using CellTiter-Glo[®] 3D cell viability assay, the IC₅₀ values of single drug were calculated by nonlinear regression, while the combination index (CI) for evaluating the drug synergy effect of the drug combination was performed by using the Chou and Talalay method in CalcuSyn software (Biosoft, Version 2.1) (Supplementary Fig. 5a). The CI values of combined PF-06409577 and Orlistat or 5Z-O in both cell lines ranged from 0.124 to 0.641, suggesting the above combined drugs exhibited synergistic anti-cancer effect on ovarian cancer cells (Supplementary Fig. 5b). Moreover, using transwell cell migration and invasion assays, knockdown of AMPK α 1 in ES-2 and OVCA433 cells further enhanced their migratory and invasive capacities by two- to sixfold in OCM (Fig. 6d). In contrast, co-treatment with either PF-06409577 or the TAK1 inhibitor 5Z-O attenuated the increased cell migratory and invasive capacities caused by AMPK α 1 knockdown in ovarian cancer cells (Fig. 6d). These results suggest that pharmaceutical activation of AMPK is equivalent to suppressing the TAK1/NF- κ B signaling activity in driving ovarian cancer cell aggressiveness in OCM.

AMPK/TAK1/NF- κ B signaling is required for metastatic seeding. To further investigate whether this AMPK/TAK1/NF- κ B signaling axis is required for promoting metastatic seeding of ovarian cancer cells in omental tissues, we established an ex vivo murine omental system by culturing omenta from 6- to 8-week-old SCID female mice (to exclude immune cells)⁵. Two highly metastatic ovarian cancer cells (ES-2 and OVCA433) were eGFP-labeled and were added to the omental culture system. The results showed that co-treatment of either the AMPK activator PF-06409577 (PF) or the TAK1 inhibitor 5Z-O could significantly inhibit tumor colony formation on the murine omenta (Fig. 7a), suggesting that the activation of AMPK or inhibition of TAK1/NF- κ B signaling could be efficient for inhibiting tumor colonization in the ex vivo omental model. We next investigated whether targeting AMPK/ACC/FASN-mediated lipogenesis and the AMPK/TAK1/NF- κ B signaling cascade suppresses ovarian cancer cell metastasis in vivo using an intraperitoneal xenograft SCID mouse model. Six days after intraperitoneal injection of ES-2 into 5–6 weeks SCID female mice, AMPK activator (PF-06409577, 20 mg/kg), FASN inhibitor (orlistat, 240 mg/kg), and TAK1 inhibitor (5Z-O, 10 mg/kg) were i.p. injected alone or as a combined cocktail for every 3 days (total of six injections) (Fig. 7b). As ES-2 is an aggressive ovarian cancer cell, it form tumors in a very short time (within 3 weeks). In the control, PF-06409577, orlistat and 5Z-O groups, five out of five mice formed tumors, while only three out of five mice had small tumor nodules in the combined cocktail group (Fig. 7c). Of note, all mice in the negative group had ascites formation, while the other groups had only 1–2 mice with ascites. Analysis of tumor weight showed that tumor-bearing mice had 70%, 60%, and 30% tumor reduction following treatment with PF-06409577, orlistat, and 5Z-O, respectively (Fig. 7d). Importantly, the combined cocktail could further reduce tumor formation up to 95% (Fig. 7d). In addition, co-treatment with either PF-06409577, orlistat or 5Z-O could suppress the number of tumor nodules compared with the negative control (Fig. 7e). As expected, the combined cocktail could completely abrogate tumor dissemination of ovarian cancer cells in the intraperitoneal cavity of mice (Fig. 7e). More importantly, by blood test, treatment with the above drugs alone or together did not cause any damage to the liver or renal functions (Table 1). Taken together, both the ex vivo omental system and in vivo tumor xenograft mouse model support our notion that targeting AMPK/ACC/FASN for lipogenesis and AMPK/TAK1/NF- κ B oncogenic signaling is able to inhibit metastatic dissemination of ovarian cancer cells in the peritoneal cavity.



Discussion

Peritoneal metastases are common, and are associated with poor prognosis, in advanced gynecological and gastrointestinal cancers²⁶. Of the different routes of peritoneal metastases, omental metastasis is the most common in early presentation of ovarian cancers²⁷. Recent evidence has suggested that adipocytes, the major cell population of the omentum, fuel ovarian cancer cell

growth and aggressiveness in colonization⁹, thus supporting the rationale for why cancer cells prefer to metastasize in lipid-enriched microenvironments or niches²⁸. In this study, we established OCM to mimic the tumor microenvironment of the intraperitoneal cavity to study its effect on tumor metabolism and oncogenic capacities¹¹. Our results revealed that ovarian cancer cells undergo metabolic reprogramming by shifting from aerobic

Fig. 3 Ovarian cancer cells cultured undergo metabolic reprogramming in OCM. **a** XTT cell proliferation assay demonstrates that 3 days of co-treatment with a glucose uptake inhibitor, STF31 (5 μ M), does not affect the growth of ovarian cancer cells cultured in OCM, whereas co-treatment of Cleanascite significantly attenuates the cell proliferation rate as compared with the effect of control OCM. **b** The uptake of glucose in OVCA433 and SKOV3 with stable knockdown of GLUT1, GLUT3, and GLUT4 by glucose uptake assay using 2-DG6P. **c** Spectrophotometric analysis and Luminescent ATP Detection Assay shows that stable knockdown of either ACC α or ACC β significantly reduces ATP production in SKOV3 and OVCA433 cells, while knockdown of GLUT1 shows slight reduction (~15–21%) of ATP production in both cell lines. **d** XTT cell proliferation assay reveals that the cell proliferation of OVCA433 and SKOV3 cells with stably knockdown of GLUT1, ACC α , and ACC β on day 3. **e** Immunofluorescent and lipid staining analyses show that the lipid droplet formation in OCM compared with DMEM control in OVCA433 cells with stably knockdown of GLUT1, ACC α , and ACC β . Scale bar = 50 μ m. **f** Transwell cell migration/invasion assays show that cell migration and invasion rates in OVCA433 cells with stably knockdown of GLUT1, ACC α , and ACC β . The stained cells were counted randomly from at least four selected fields and the representative images with bar charts were shown. Scale bar = 50 μ m. **g** Effects of GLUT1 or ACC α knockdown on ovarian cancer dissemination in xenograft mouse tumor model. SKOV3 cells with either GLUT1 (shGLUT1) or ACC α (shACC α) knockdown were injected into the intraperitoneal cavity of 5–6-week-old SCID female mice ($n = 5$). Scrambled control (SC) shRNA is used as a negative control ($n = 5$). Tumor nodule formation and localization are shown (red arrow); imaged were captured on day 45 after cancer cell inoculation. The bar chart indicates that the average tumor weight of the shACC α and shGLUT1 experimental groups are significantly lower than the SC groups. Results were presented as mean \pm S.E.M. Data were analyzed by Student's *t*-tests or one-way/two-way ANOVA with Tukey's post hoc test (* $p < 0.05$, ** $p < 0.01$, *** $p < 0.001$, **** $p < 0.0001$)

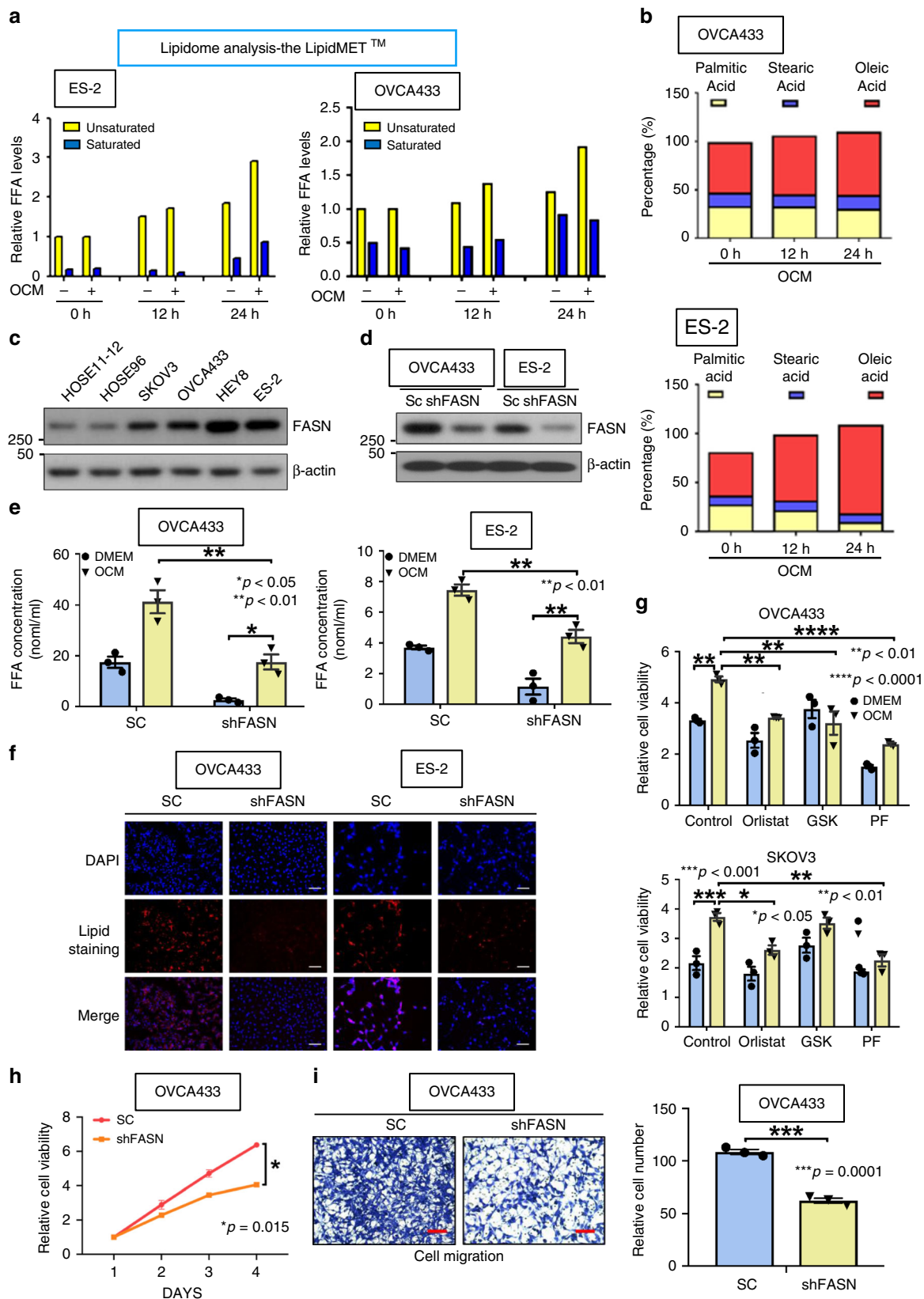
glycolysis to fatty acid oxidation to produce ATP and thus support their increased cell proliferation and enhanced cell migration/invasion capacities in the fatty acid-enriched OCM. We further found that AMPK acts as a key energy regulator in controlling ACC in lipogenesis and elevated lipolysis and β -oxidation activities. On the other hand, the high ATP production from β -oxidation suppressed AMPK activity, which in turn, liberated the inhibition of mTOR activity and promoted cancer cell growth²⁹. Importantly, we are the first to demonstrate that TAK1/NF- κ B signaling, as the dominant downstream signaling pathway, is similar to mTOR signaling, inversely modulated by AMPK activity, and involved in ovarian cancer aggressiveness in the intraperitoneal cavity or ascites microenvironment.

Metabolic reprogramming has been recently recognized as another hallmark of cancer because it is critical for cancer metastatic progression and minimal residual disease³⁰. Tumor tissues are known to be composed of not only cancer cells but also other cell types, indicating that cancer cells are surrounded by heterogeneous intratumoral backgrounds³¹. Thus, genetic/epigenetic alterations during tumor development cause cancer cells to possess the capacity of cellular metabolic heterogeneity or metabolic symbiosis in order to adapt and develop during drastic changes in the nutrient microenvironment³². The Warburg effect is a distinct feature of many human cancers that allows cells to exhibit enhanced aerobic glycolysis to generate energy for their rapid cell proliferation under stress conditions³³. However, ascites provide a distinct tumor microenvironment that affects ovarian cancer cells in different aspects and associates with peritoneal metastases and poor prognosis³⁴. Malignant ascites act as a reservoir of a complex mixture of bioactive lipids, pro-inflammatory factors and a tumor-promoting microenvironment for metastatic progression of ovarian cancer cells^{35,36}. The high free fatty acid content in ascitic fluid provides a huge energy source and may force ovarian cancer cells to undergo metabolic reprogramming from aerobic glycolysis to fatty acid β -oxidation to produce energy for tumor growth. Indeed, our findings showed that ovarian cancer cells conduct lipogenesis and fatty acid β -oxidation for cellular blocks synthesis and ATP production. On the other hand, the inhibition of glycolysis using STF31³⁷, or shRNAi targeted at GLUT1³⁸, could not alter ovarian cancer cell proliferation or cell migration/invasion when co-cultured in OCM. By contrast, knockdown of ACC α and/or ACC β not only impaired lipogenesis but also fatty acid β -oxidation for ovarian cancer cell proliferation and cell migration/invasion of ovarian cancer cells cultured in OCM. These data indicate the metabolic plasticity of ovarian cancer cells in the adaptation of abundant availability of free fatty acids in ascites or omental tissues induce

ovarian cancer cells to shift glycolysis to lipid metabolism for ATP production to sustain their cell survival and tumor progression^{39,40}.

AMPK is a key energy sensor that not only maintains the balance of energy consumption and expenditure but also modulates cell protection against stresses and cell proliferation^{41,42}. Thus, AMPK activity should be increased in ovarian cancer cells under the hypoxic ascites microenvironment because of pathogenic stresses and low oxygen content. However, it is well known that sustained high AMPK activity may inhibit mTOR signaling in tumor growth⁴³. In fact, as cancer cells prefer low AMPK for tumor development and metastasis, low AMPK levels commonly occur in advanced cancer cells because genetic/epigenetic progression enhances cell tolerance to stress and increases cell growth and aggressiveness^{44,45}. Our study showed that ovarian cancer cells initially displayed high AMPK activity because of the change in the culture conditions from DMEM to a fatty acid-enriched medium. The high AMPK activity could protect cells against stresses from different media; however, importantly, switching to lipogenesis and lipolysis could have also had a protective effect on ovarian cancer cells. Interestingly, we found that there is an inverse relationship between ATP production and AMPK activity in ovarian cancer cells, suggesting that there is a negative feedback loop to suppress AMPK activity after prolonged culture in OCM⁴³. As a result, the combination of high ATP and low AMPK activity synergistically enhances ovarian cancer aggressiveness in OCM. Previous investigations have noted that low AMPK activity favors tumor progression and invasion^{46,47}. Consistently, our findings using knockdown of AMPK α in ovarian cancer cells confirmed that low AMPK activity is required for ex vivo and in vivo tumor growth.

Emerging evidence has suggested AMPK modulates numerous downstream signaling pathways for cell survival and other properties^{48,49}. This indicates the suppression of mTOR signaling is not sufficient to account for the effect of low AMPK in promoting ovarian cancer aggressiveness. Indeed, we previously reported that TAK1/NF- κ B signaling plays a critical role in enhancing ovarian cancer tumorigenicity in OCM¹¹. Although it's controversial that TAK1 may act as the upstream or downstream target of AMPK^{50,51}, our findings have confirmed that TAK1/NF- κ B signaling, in line with mTORC1, is negatively regulated by AMPK in ovarian cancer cells. Therefore, inhibition of TAK1/NF- κ B signaling by 5Z-O or suppression of AMPK/ACC/FASN signaling in lipogenesis by the potent AMPK activator PF-06409577⁵² or orlistat could inhibit ovarian cancer dissemination and tumor growth in vivo. Importantly, we found that a combined cocktail of the above reagents could further exert



synergistic anti-cancer effects in 3D spheroids culture in vitro and metastatic dissemination in vivo. Previous studies have shown that low dosage of PF-06409577²⁵, orlistat⁵³, and 5Z-O⁵⁴ exhibit low toxicity in vitro and in vivo. Indeed, a blood test for renal and liver functions in mice that received the same dose and time

intervals of the above reagents revealed no sign of toxicity in the mice. This indicates these reagents exert no toxicity in vivo, at least in low doses.

In summary, dynamic metabolic alterations occur in advanced stage ovarian cancer cells to adapt to drastic changes in the

Fig. 4 Ovarian cancer cells undergo lipogenesis in OCM. **a** The bar chart shows the Lipidomic analysis of the amount of intercellular unsaturated and saturated fatty acids in two ovarian cancer cells which were cultured in OCM from 0 to 24 h. The DMEM is used as a negative control. The Lipidomic analysis was performed by Metabo-Profile, Shanghai, China. **b** The percentage bar chart shows the changes of the major unsaturated fatty acid, Oleic acid, and two saturated fatty acids, Stearic acid and Palmitic acids in OVCA433 and ES-2 cells cultured in OCM from 0 to 24 h. **c** Western blot analysis compares the expression level of a key lipogenic enzyme, FASN, in two HOSEs and four ovarian cancer cell lines, SKOV3, OVCA433, Hey8, and ES-2. **d** Western blot analysis shows the reduction of FASN knockdown by lentiviral shRNAi approach in OVCA433 and ES-2. **e** Free fatty acid assay demonstrates the depletion of FASN leads to the reduction of long chain fatty acid (>8 carbon) in OVCA433 and ES-2 cells when cultured in DMEM or OCM. **f** Lipid droplet formation assay reveals the formation of lipid droplets in FASN knockdown OVCA433 and ES-2 cells as compared with their scrambled controls (SC). Scale bar = 50 μ m. **g** XTT cell proliferation assay shows that 3 days of co-treatment with the above FASN inhibitors, orlistat (30 μ M) and GSK2194069 (100 nM) (GSK), or AMPK activator, PF-06409577 (50 μ M) (PF), significantly reduces the OCM-induced cell growth rate in SKOV3 and OVCA433 cells. **h** XTT cell proliferation assay reveals that the cell proliferation of OVCA433 with or without FASN knockdown co-cultured in OCM for 4 days. **i** Transwell cell migration assay shows the cell migratory rate of OVCA433 with or without FASN knockdown co-cultured in OCM for 12 h. The stained cells were counted from three selected fields randomly. Representative images and quantitative results of cell migration were shown. Scale bar = 50 μ m. Results were presented as mean \pm S.E.M. Data were analyzed by Student's *t*-tests or one-way/two-way ANOVA with Tukey's post hoc test (* p < 0.05, ** p < 0.01, *** p < 0.001, **** p < 0.0001)

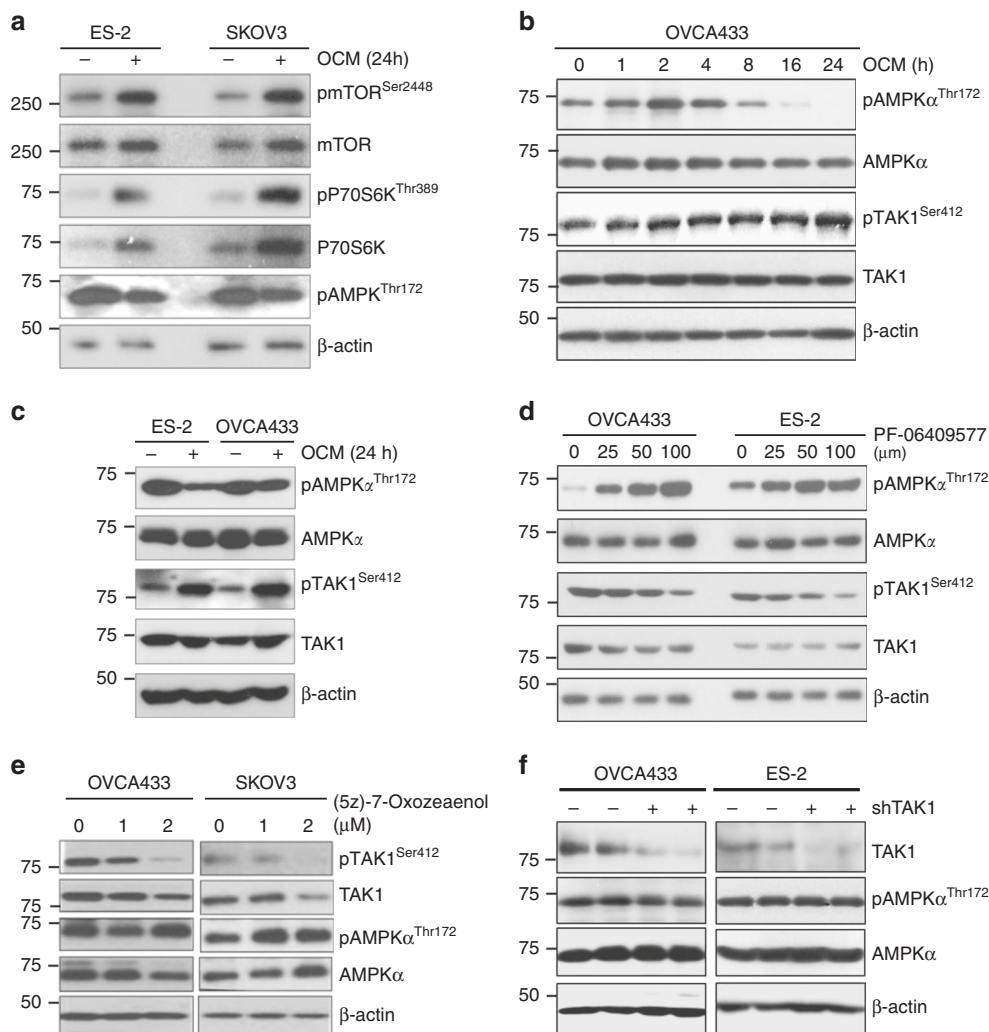


Fig. 5 Oncogenic pathways regulated by AMPK in ovarian cancer cells. **a** Long-term culture with OCM (24 h) leads to reduction in AMPK activity (pAMPK^{Thr172}), activation of mTOR activity (pmTOR^{Ser2448}), and increased phosphorylation of p70S6K (pP70S6K^{Thr389}) in ES-2 and SKOV3 cells. **b** While culturing OVCA433 cells in OCM for 24 h leads to downregulation of pAMPK^{Thr172}, but elevation of the level of pTAK^{Ser412}. **c** Long-term culture with OCM (24 h) with ES-2 and OVCA433 causes an inverse relationship between the AMPK (reduced pAMPK^{Thr172}) and TAK1 (increased pTAK^{Ser412}) activities. **d** The level of pAMPK^{Thr172} is increased, while the level of pTAK^{Ser412} is reduced upon treatment with AMPK activator, PF-06409577 (24 h), in a dose-dependent manner in OVCA433 and ES-2 ovarian cancer cells. **e** Co-treatment with TAK1 inhibitor, (5Z)-7-Oxozeaenol (2.5 μ M), substantially inhibits the expression of pTAK^{Ser412} in a dose-dependent manner (24 h), and this effect is accompanied by an increase in pAMPK^{Thr172} levels in OVCA433 and SKOV3 cells. **f** Knockdown of endogenous TAK1 by shRNAi more than 70% does not alter either pAMPK^{Thr172} or total AMPK in OVCA433 cells

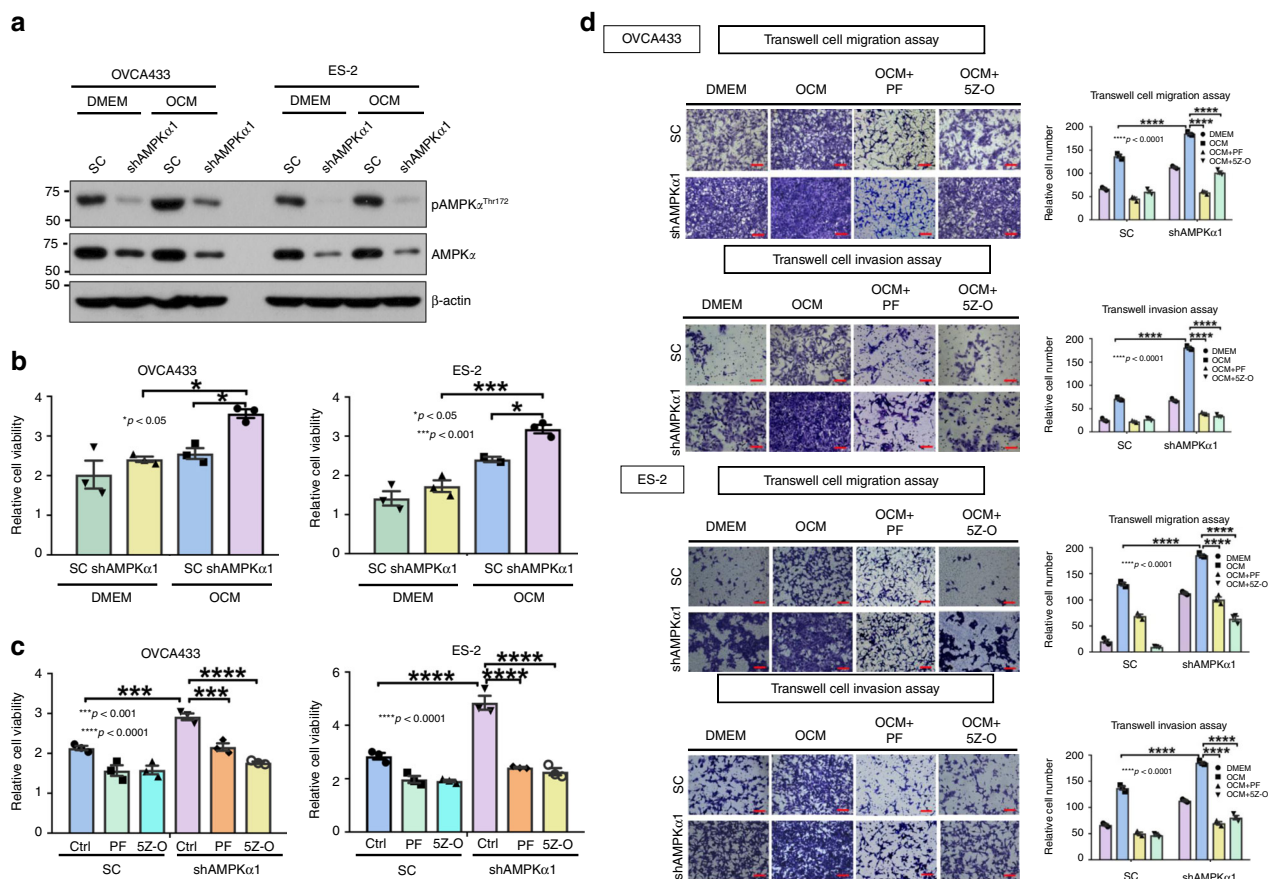


Fig. 6 Targeting AMPK or inhibiting TAK1 signaling activity impairs ovarian cancer aggressiveness. **a** AMPK α 1 knockdown stable clones were established via shRNA lentiviral approach targeting the α 1-isoform of AMPK in OVCA433 and ES-2 cells, and cells cultured in DMEM or OCM (2 h) could not induce AMPK activity (pAMPK^{Thr172}) in shAMPK α 1 clones compared with their scrambled controls (SC) of both cell lines. **b** XTT cell proliferation assay shows that OCM can promote proliferation of ES-2 and OVCA433 cells, but after depletion of AMPK α 1 in both cell lines, shAMPK α 1 clones show significantly higher cell proliferation than that of scrambled controls (SC) cultured in DMEM or OCM for 3 days. **c** XTT cell proliferation assay shows that 3 days of co-treatment with AMPK activator PF-06409577 (50 μ M) (PF) or TAK1 inhibitor (5Z)-7-Oxozeanol (2.5 μ M) (5Z-O) significantly inhibited cell proliferation in both parental and AMPK α knockdown clones compared with the scrambled controls (SC) of ES-2 and OVCA433 cells. **d** Transwell cell migration/invasion assays demonstrate that the cell migratory and invasive capacities of OVCA433 and ES-2 cells are enhanced by OCM. Knockdown of AMPK α 1 further promotes the migration and invasion rates of cells cultured in OCM or DMEM. In contrast, co-treatment with AMPK activator PF-06409577 (50 μ M) (PF) or TAK1 inhibitor 5Z-O (2.5 μ M) somewhat abrogated the cell migratory and invasive capacities of AMPK α 1 knockdown clones and scrambled controls (SC) of both cell lines. The stained cells were counted at least from four randomly selected fields. Representative images and quantitative results were shown by bar charts. Scale bar = 50 μ m

nutrient microenvironment. In this study, ovarian cancer cells utilize lipid metabolism in the ascites or omental microenvironment during metastatic progression through AMPK/ACC/FASN-mediated lipogenesis and AMPK/TAK1/NF- κ B signaling cascades. Hence, targeting these pathways by a combined cocktail of low-toxic compounds may be an alternative therapeutic intervention to impede ovarian cancer peritoneal metastases.

Methods

Ovarian cancer samples and cell lines. Ovarian cancer cell lines A2780cp and SKOV3 (high-grade ovarian cancer cell lines) and ES-2 (kindly provided by Prof. Benjamin Tsang, University of Ottawa), Hey8 (Prof. Alice Wong, The University of Hong Kong) and OVCA433 (Prof. George Tsao, The University of Hong Kong) (high-grade serous subtype)^{55,56} were all cultured in Dulbecco's-modified Eagle medium (DMEM) (Gibco-BRL, Minneapolis, MN, USA) supplemented with 10% heat-inactivated fetal bovine serum (FBS) (Gibco-BRL) and penicillin/streptomycin (100 units/mL); cells were incubated at 37 °C with an atmosphere of 5% CO₂. In-house short tandem repeat (STR) DNA profiling analysis was used to authenticate the above cell lines, and mycoplasma contamination was also assessed. Freshly collected peritoneal fluids or ascites, ovarian tumor specimens and omental tissues were surgically resected from ovarian cancer patients of Queen Mary Hospital. The

use of these clinical samples in this study was approved by the Institutional Review Board of the University of Hong Kong/Hospital Authority Hong Kong West Cluster (HKU/HA HKW IRS) (IRS Reference Number: UW 11-298).

OCM and commercial kits. Freshly resected omental tissues from ovarian cancer patients were directly collected during the operation at Queen Mary Hospital and delivered to our laboratory within 2 h. The omental tissue was washed in PBS and minced into pieces at similar size. After transferring into 1% DMEM, omental mixture was incubated at 37 °C with 5% CO₂ for 24 h. Then all the omental tissue was removed on the following day by a SPL cell strainer (Bio Lab, Conyers, GA, USA), followed by centrifugation at 1500 \times g for 5 min for three times. Finally, the OCM was accomplished after filtration the supernatant medium 0.7 μ m column filter. For storage, e.g., 1 month, OCM was aliquoted and stored at 4 °C for further study. Cleanascite™ Lipid Removal Reagent (Biotech Support Group, Monmouth Junction, NJ, USA) was used for selectively removing lipoproteins, lipids, floating fats, and cell debris without affecting other serum components including hormones in OCM or ascites. 2-DG (equivalent to glucose) was taken up by glucose transporters and metabolized to 2-DG-6-phosphate (2-DG6P). The other kits and drugs used in this study are shown in Supplementary Table 1.

Stable cell transfection and cell sorting. Stable knockdown clones for AMPK α , GLUT1, GLUT3, GLUT4, ACC α , and ACC β of ovarian cancer cells were established by lentiviral shRNAi-mediated particles (Santa Cruz, Dallas, Texas, USA) and selected with 1 μ g/10 mL puromycin for 2 weeks. The efficiency of transfection

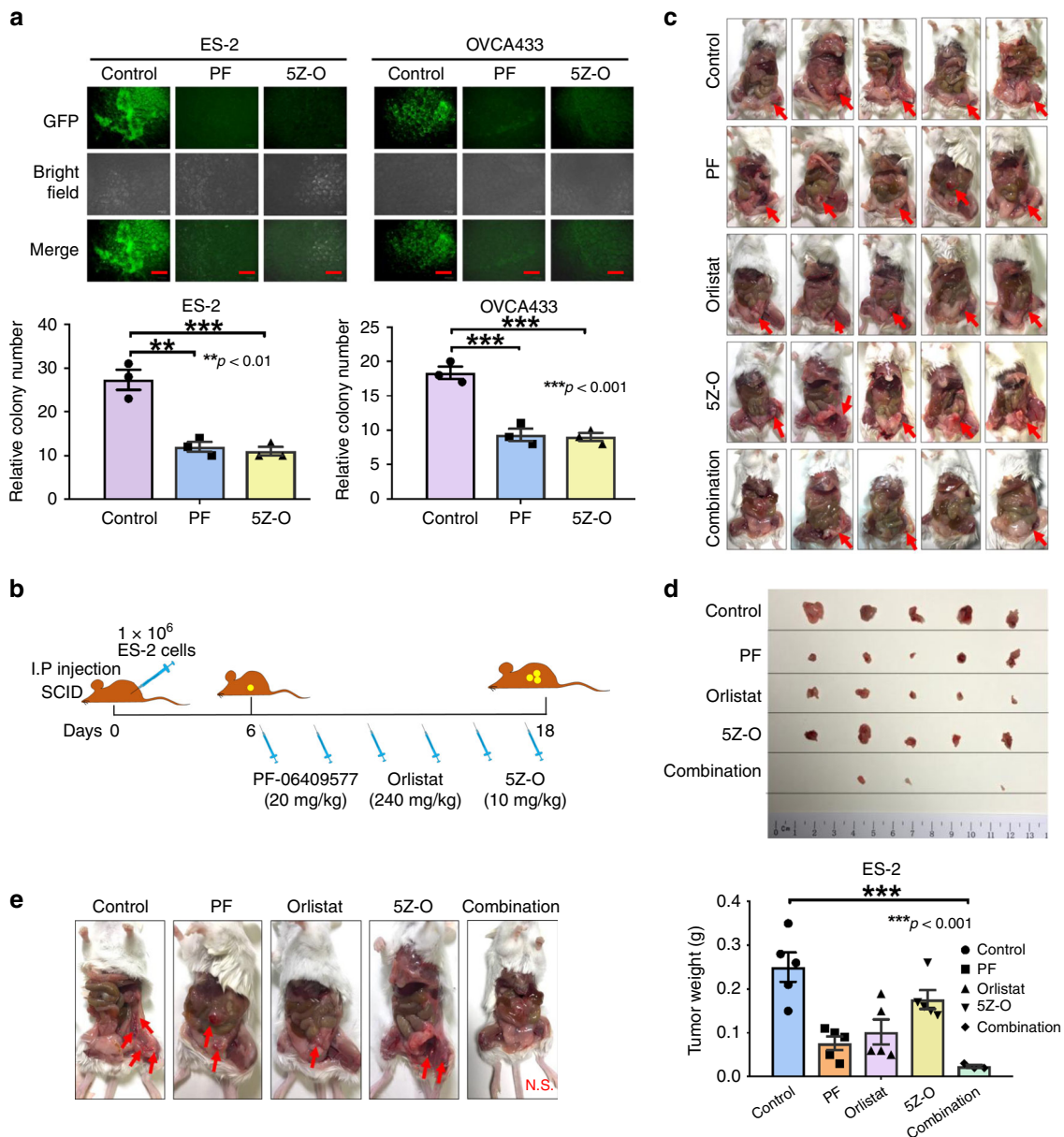


Fig. 7 AMPK/FASN/TAK1/NF- κ B signaling axis is required for metastatic colonization. **a** eGFP-labeled ES-2 and OVCA433 ovarian cancer cells were established by infection with LV-CMV-RLuc-IRES-GFP lentiviral particles. After incubating GFP-labeled ovarian cancer cells with omental tissues from 6- to 8-week-old SCID female mice, the results show that ES-2 and OVCA433 cells exhibit a significant number of tumor colonies on murine omenta on day 30. However, co-treatment with AMPK activator PF-06409577 (50 μ M) (PF) or TAK1 inhibitor 5Z-O (2.5 μ M), remarkably reduces the number and size of tumor colonies by 45–55% on the murine omenta. Scale bar = 100 μ m. **b** Schematic overview showing the experimental protocol of the anti-tumorigenic effect of the combined cocktail of the AMPK activator PF-06409577 (20 mg/kg), FASN inhibitor orlistat (240 mg/kg), and TAK1 inhibitor 5Z-O (10 mg/kg) on ovarian cancer cells in SCID mice. ES-2 cells ($1 \times 10^6/200 \mu$ l) were injected into the intraperitoneal cavity of 5–6-week-old SCID female mice. On day 6, the above three drug reagents were injected individually or in combination (for a total of six injections) from day 6 to day 18. **c** Images show tumor formation in all mice. **d** Images showing tumor nodules obtained from all mice. The bar chart shows the average tumor weight obtained from each group. **e** Representative images showing the number and locations of tumor nodules distributed in the intraperitoneal cavity of each mouse group. Results were presented as mean \pm S.E.M. Data were analyzed by one-way ANOVA with Tukey's post hoc test (* $p < 0.05$, ** $p < 0.01$, *** $p < 0.001$, **** $p < 0.0001$)

was verified by western blot analysis. To achieve eGFP-labeling cells, LV-CMV-RLuc-IRES-GFP pre-made lentiviral particles containing luciferase and GFP reporters (Capital Biosciences, Rockville, MD, USA) were infected into shAMPK α knockdown ovarian cancer cells. Cell sorting for high fluorescence was performed on transfectants by using a BD FACSARIA I Cell Sorter (Faculty Core Facility, The University Hong Kong).

Proteomics, lipidomics, and bioinformatics analysis. LC-MS/MS analysis was carried out on an Orbitrap Fusion Lumos mass spectrometer interfaced with

Dionex 3000RSLC nanoLC. The high resolution, high mass accuracy MS data obtained were processed using Maxquant version 1.5.3.30, in which MS data analyzed in triplicates for each condition were searched using the Andromeda algorithm against Uniprot Human protein database. Appropriate parameter settings to obtain peptide and protein data using 0.1% FDR at peptide and protein level. Data visualization and statistical data analysis were performed by Perseus software version 1.5.4.1. Differential proteins were subjected to Gene Ontology enrichment analysis using PANTHER⁵⁸, and Ingenuity pathway analysis (IPA) software (Qiagen Bioinformatics). The fatty acid profiling in ovarian cancer cells co-cultured in OCM and DMEM control was performed by using FFA Kit Ultra on

Table 1 Table showing the renal and liver function tests of two groups of SCID mice and control and drug combined cocktail tests

Animal	Control	Drug combination	Reference range
<i>Liver function</i>			
Bilirubin total	0.7	0.6	0.1–0.9 mg/dL
Bilirubin direct	0.6	0.6	0.1–1.2 mg/dL
Alkaline phosphatase	200	122	62–209 U/L
Protein total	5.2	4.9	3.6–3.3 mg/dL
ALT	45	54	28–132 U/L
AST	76	100	59–247 U/L
<i>Renal function</i>			
Albumin	2.8	2.5	2.5–4.8 g/dL
Calcium	10	10.2	5.9–9.4 mg/dL
Chloride	113	110	92–120 mmol/L
Creatinine	<0.30	<0.30	0.20–0.80 mg/dL
Glucose	112	141	90–192 mg/dL
Phosphorus	10.3	10.3	6.1–10.1 mg/dL
Potassium	6.5	6.5	4.6–8.0 mmol/L
Sodium	148	144	124–174 mmol/L
BUN	19.5	16	18–29 mg/dL

an ultra-performance liquid chromatography coupled to tandem-mass spectrometry (UPLC-MS/MS) system (Metabo-Profile, Shanghai, China).

Western blot analysis. Western blot analysis was performed as previously described⁵⁷. Briefly, the protein lysates were isolated using cell lysis buffer (Cell Signaling Technology), and separated by 10% SDS-PAGE before transferring to polyvinylidene difluoride (PVDF) membranes. The membranes were then pre-blotted with 5% skimmed milk and followed by probing with primary antibodies. The list of primary antibodies used in this study are available in Supplementary Table 2. The goat anti-rabbit or anti-mouse secondary antibody with horseradish peroxidase-conjugated (Amersham, Uppsala, Sweden) were added. Immunodetection was carried out using ECLTM Western Blotting Detection Reagents (Bio-Rad) and visualized by X-ray film.

Fluorescent staining. Fluorescent staining on the lipid droplet in the ovarian cancer cells were performed using Nile Red (Molecular Probes, Eugene, OR, USA) according to the manufacturer's protocol⁵⁹. Cells were seeded in 6-well plate in which a sterile glass coverslip had been placed in advance. After 24 h starvation, cells were treated with OCM or DMEM with 1% FBS for 24 h in the same condition as cell culture. Four percent paraformaldehyde (PFA) was used to fix the cell, and followed by the incubation of Nile Red at a concentration of 1 µg/10 mL 150 mM NaCl for 30 min. Then the coverslip was placed on a microslide with a drop of FluoroshieldTM with DAPI (Sigma-Aldrich, St. Louis, MO, USA) to stain cell nucleus. Inner lipid droplet of ovarian cancer cells was stained into red color while nucleus was stained into blue. Cells were captured by Nikon eclipse Ti-S (Nikon, Tokyo, Japan) fluorescent microscope or Zeiss LSM 780 confocal microscope (Carl Zeiss, Germany). To quantify the fluorescent signal of the lipid droplets, three cells per visual field were randomly selected. Measurements of fluorescence intensity were performed by Carl Zeiss ZEN 2.3 Version 13.0.0.0, with normalization of cytosolic intensity. Mean signal intensities were obtained from at least five visual fields.

XTT cell proliferation, transwell cell migration/invasion assays. Cell viability or cell growth was evaluated by cell proliferation kit (XTT) (Roche Diagnostics, Indianapolis, USA). Briefly, cells were separately seeded in 96-well plates and were treated with OCM added with 1% FBS for different duration of day. To avoid bias, triplicate wells were performed. A mixture of XTT reagent, which contains PBS, XTT labeling reagent, and electron coupling reagent, was incubated with each well for 4 h at 37 °C. Then the absorbance of each well at 492 nm was detected. The relative cell viability was calculated as a fold change relative to the mean of the first day. The capacities of cell migration and invasion of ovarian cancer cell were performed by Transwell cell migration and invasion assay kit (Merck Millipore, New Orleans, LA, USA) according to the manufacturer's protocol and pictured by microscopy. Relative migratory cell numbers were counted at least from three randomly chosen.

Three-dimensional (3D) cell culture drug-sensitivity assay. Ovarian cancer cells were suspended in OCM containing 2% GeltrexTM Matrix (Gibco-BRL, Gaithersburg, MD) and seeded in the NunclonTM SpheraTM 96U-microplates (Thermo Fisher Scientific Inc., Waltham, Massachusetts) with the super low cell attachment

surface at around 2000 cells/well density in triplicate. Cells were subsequently allowed to grow for 1 week before treatments with each indicated drug at serial diluted concentrations or in combination for 72 h. After the corresponding drug treatments, viable cells were detected by luminescent cell viability assay using CellTiter-Glo[®] 3D cell viability assay (Promega Corporation, Madison, WI).

Ex vivo omental colonization assay. The procedure of this assay was modified from a previous study⁵. Omentum was surgically resected from sacrificed 6–8-week-old SCID female mice and was placed in pre-cooled PBS. Cells were trypsinized and re-suspended in a concentration of $3 \times 10^5/2$ mL in DMEM/F12 (Gibco-BRL, Grand Island, NY, USA) with 20% FBS. Omental tissue was cut into even-sized pieces and spread out drily at the bottom of each well of plate. Two milliliters of cell suspension was added to each well and was incubated at 37 °C and 5% CO₂ for 24 h. Then the omentum was removed out and placed into a 6-well plate, washing with PBS gently to discard the non-attached cells. Each well was cultured with DMEM/F12 with 20% FBS, and the medium was changed for every 3 days. After 14 days of incubation, ZOETM Fluorescent Imager (Bio-Rad, Hercules, CA, USA) was used to visualize and captured the tumor nodule formation in omentum.

In vivo intraperitoneal dissemination mouse model. A highly metastatic ovarian cancer cell line ES-2⁶⁰ was selected for labeling by transfecting the LV-CMV-RLuc-IRES-GFP plasmid (consists of both luciferase and GFP reporters) (Capital Biosciences, Inc., Rockville, MD, USA). Then, the eGFP-labeled ES-2 (1×10^6 cells/200 µL) cells were intraperitoneally (i.p.) injected into 5–6-week-old SCID female mice. Tumor dissemination was observed by a laparotomy procedure^{61,62}. Metastatic tissues were examined by histological examination using H&E staining. Blood samples were collected from the facial vein via puncture at the rear of the jawbone. All blood tests for renal and liver function analyses were performed by PathLab Medical Laboratories Ltd. (Hong Kong). All animal experiments were approved by the University of Hong Kong Committee on the Use of Live Animals in Teaching and Research (CULATR No. 3968-16).

Statistical analysis. All statistical analyses were performed by GraphPad Prism 5.0 (San Diego, CA, USA). Data were analyzed by unpaired *t*-test, and one/two-way analysis of variance (ANOVA) followed by Tukey post hoc comparison. All data were obtained from at least three independent experiments, each performed in triplicate, and data are expressed as mean ± S.E.M. and *p* < 0.05 was considered as statistically significant.

Reporting summary. Further information on research design is available in the Nature Research Reporting Summary linked to this article.

Data availability

The proteomic array, lipidomic profiling datasets, and the source data of charts in the current study are available in figshare^{63–65}.

Received: 27 November 2018 Accepted: 20 June 2019

Published online: 31 July 2019

References

- Roett, M. A. & Evans, P. Ovarian cancer: an overview. *Am. Fam. Physician* **80**, 609–616 (2009).
- Bristow, R. E., Tomacruz, R. S., Armstrong, D. K., Trimble, E. L. & Montz, F. J. Survival effect of maximal cytoreductive surgery for advanced ovarian carcinoma during the platinum era: a meta-analysis. *J. Clin. Oncol.* **20**, 1248–1259 (2002).
- Vergote, I. et al. Neoadjuvant chemotherapy or primary surgery in stage IIIC or IV ovarian cancer. *New Engl. J. Med.* **363**, 943–953 (2010).
- Clark, R. et al. Milky spots promote ovarian cancer metastatic colonization of peritoneal adipose in experimental models. *Am. J. Pathol.* **183**, 576–591 (2013).
- Khan, S. M. et al. In vitro metastatic colonization of human ovarian cancer cells to the omentum. *Clin. Exp. Metastas.* **27**, 185–196 (2010).
- Bainer, R. O. et al. Time-dependent transcriptional profiling links gene expression to mitogen-activated protein kinase 4 (MKK4)-mediated suppression of omental metastatic colonization. *Clin. Exp. Metastas.* **29**, 397–408 (2012).
- Kim, S., Kim, B. & Song, Y. S. Ascites modulates cancer cell behavior, contributing to tumor heterogeneity in ovarian cancer. *Cancer Sci.* **107**, 1173–1178 (2016).
- Ghoneum, A., Afify, H., Salih, Z., Kelly, M. & Said, N. Role of tumor microenvironment in ovarian cancer pathobiology. *Oncotarget* **9**, 22832–22849 (2018).

9. Nieman, K. M. et al. Adipocytes promote ovarian cancer metastasis and provide energy for rapid tumor growth. *Nat. Med.* **17**, 1498–1503 (2011).
10. Leinster, D. A. et al. The peritoneal tumour microenvironment of high-grade serous ovarian cancer. *J. Pathol.* **227**, 136–145 (2012).
11. Cai, P. C. et al. Elevated TAK1 augments tumor growth and metastatic capacities of ovarian cancer cells through activation of NF- κ B signaling. *Oncotarget* **5**, 7549–7562 (2014).
12. Kumar, A., Wong, A. K., Tizard, M. L., Moore, R. J. & Lefevre, C. miRNA_Targets: a database for miRNA target predictions in coding and non-coding regions of mRNAs. *Genomics* **100**, 352–356 (2012).
13. Menendez, J. A. Fine-tuning the lipogenic/lipolytic balance to optimize the metabolic requirements of cancer cell growth: molecular mechanisms and therapeutic perspectives. *Biochim. Biophys. Acta Mol. Cell Biol. Lipids* **1801**, 381–391 (2010).
14. Carling, D., Mayer, F. V., Sanders, M. J. & Gamblin, S. J. AMP-activated protein kinase: nature's energy sensor. *Nat. Chem. Biol.* **7**, 512–518 (2011).
15. Viollet, B. et al. AMPK inhibition in health and disease. *Crit. Rev. Biochem. Mol. Biol.* **45**, 276–295 (2010).
16. Taylor, S. W., Clarke, N. J., Chen, Z. & McPhaul, M. J. A high-throughput mass spectrometry assay to simultaneously measure intact insulin and C-peptide. *Clin. Chim. Acta* **455**, 202–208 (2016).
17. Koppenol, W. H., Bounds, P. L. & Dang, C. V. Otto Warburg's contributions to current concepts of cancer metabolism. *Nat. Rev. Cancer* **11**, 325–337 (2011).
18. Grunt, T. W. Interacting cancer machineries: cell signaling, lipid metabolism, and epigenetics. *Trends Endocrinol. Metab.* **29**, 86–98 (2018).
19. Kridel, S. J. & Lowther, W. T. Pemble CWt. Fatty acid synthase inhibitors: new directions for oncology. *Expert Opin. Investig. Drugs* **16**, 1817–1829 (2007).
20. Veigel, D. et al. Fatty acid synthase is a metabolic marker of cell proliferation rather than malignancy in ovarian cancer and its precursor cells. *Int. J. Cancer* **136**, 2078–2090 (2015).
21. Ducharme, N. A. & Bickel, P. E. Lipid droplets in lipogenesis and lipolysis. *Endocrinology* **149**, 942–949 (2008).
22. Hardie, D. G. AMPK and Raptor: matching cell growth to energy supply. *Mol. Cell* **30**, 263–265 (2008).
23. Lipner, M. B. et al. Metformin treatment does not inhibit growth of pancreatic cancer patient-derived xenografts. *PLoS One* **11**, e0147113 (2016).
24. Populo, H., Lopes, J. M. & Soares, P. The mTOR signalling pathway in human cancer. *Int. J. Mol. Sci.* **13**, 1886–1918 (2012).
25. Cameron, K. O. et al. Discovery and preclinical characterization of 6-Chloro-5-[4-(1-hydroxycyclobutyl)phenyl]-1H-indole-3-carboxylic Acid (PF-06409577), a direct activator of adenosine monophosphate-activated protein kinase (AMPK), for the potential treatment of diabetic nephropathy. *J. Med. Chem.* **59**, 8068–8081 (2016).
26. Hasovits, C. & Clarke, S. Pharmacokinetics and pharmacodynamics of intraperitoneal cancer chemotherapeutics. *Clin. Pharmacokinet.* **51**, 203–224 (2012).
27. Lengyel, E. Ovarian cancer development and metastasis. *Am. J. Pathol.* **177**, 1053–1064 (2010).
28. Silva, J. et al. Lipids isolated from bone induce the migration of human breast cancer cells. *J. Lipid Res.* **47**, 724–733 (2006).
29. Taliaferro-Smith, L. et al. LKB1 is required for adiponectin-mediated modulation of AMPK-S6K axis and inhibition of migration and invasion of breast cancer cells. *Oncogene* **28**, 2621–2633 (2009).
30. Hilvo, M. et al. Accumulated metabolites of hydroxybutyric acid serve as diagnostic and prognostic biomarkers of ovarian high-grade serous carcinomas. *Cancer Res.* **76**, 796–804 (2016).
31. Faquin, W. C., Fitzgerald, J. T., Boynton, K. A. & Mutter, G. L. Intratumoral genetic heterogeneity and progression of endometrioid type endometrial adenocarcinomas. *Gynecol. Oncol.* **78**, 152–157 (2000).
32. Yoshida, G. J. Metabolic reprogramming: the emerging concept and associated therapeutic strategies. *J. Exp. Clin. Cancer Res.* **34**, 111 (2015).
33. Icard, P., Kafara, P., Steyaert, J. M., Schwartz, L. & Lincet, H. The metabolic cooperation between cells in solid cancer tumors. *Biochim. Biophys. Acta Mol. Cell Biol. Lipids* **1846**, 216–225 (2014).
34. Yagi, H., Yotsumoto, F. & Miyamoto, S. Heparin-binding epidermal growth factor-like growth factor promotes transcoelomic metastasis in ovarian cancer through epithelial-mesenchymal transition. *Mol. Cancer Ther.* **7**, 3441–3451 (2008).
35. Yamada, T. et al. Lysophosphatidic acid (LPA) in malignant ascites stimulates motility of human pancreatic cancer cells through LPA1. *J. Biol. Chem.* **279**, 6595–6605 (2004).
36. Pua, T. L., Wang, F. Q. & Fishman, D. A. Roles of LPA in ovarian cancer development and progression. *Future Oncol.* **5**, 1659–1673 (2009).
37. Chan, D. A. et al. Targeting GLUT1 and the Warburg effect in renal cell carcinoma by chemical synthetic lethality. *Sci. Transl. Med.* **3**, 94ra70 (2011).
38. Gu, J. et al. Correlation of GLUT-1 overexpression, tumor size, and depth of invasion with 18F-2-fluoro-2-deoxy-D-glucose uptake by positron emission tomography in colorectal cancer. *Dig. Dis. Sci.* **51**, 2198–2205 (2006).
39. Schwartz, B. & Yehuda-Shnaidman, E. Putative role of adipose tissue in growth and metabolism of colon cancer cells. *Front. Oncol.* **4**, 164 (2014).
40. Nieman, K. M., Romero, I. L., Van Houten, B. & Lengyel, E. Adipose tissue and adipocytes support tumorigenesis and metastasis. *Biochim. Biophys. Acta Mol. Cell Biol. Lipids* **1831**, 1533–1541 (2013).
41. Hardie, D. G. & Ashford, M. L. AMPK: regulating energy balance at the cellular and whole body levels. *Physiology* **29**, 99–107 (2014).
42. Hardie, D. G. AMPK: a target for drugs and natural products with effects on both diabetes and cancer. *Diabetes* **62**, 2164–2172 (2013).
43. Hardie, D. G. The AMP-activated protein kinase pathway—new players upstream and downstream. *J. Cell Sci.* **117**, 5479–5487 (2004).
44. Li, W., Saud, S. M., Young, M. R., Chen, G. & Hua, B. Targeting AMPK for cancer prevention and treatment. *Oncotarget* **6**, 7365–7378 (2015).
45. Hardie, D. G. Molecular pathways: is AMPK a friend or a foe in cancer? *Clin. Cancer Res.* **21**, 3836–3840 (2015).
46. Faubert, B. et al. AMPK is a negative regulator of the Warburg effect and suppresses tumor growth in vivo. *Cell Metab.* **17**, 113–124 (2013).
47. Li, C. et al. Reduced expression of AMPK-beta1 during tumor progression enhances the oncogenic capacity of advanced ovarian cancer. *Mol. Cancer* **13**, 49 (2014).
48. Salminen, A., Hyttinen, J. M. & Kaarniranta, K. AMP-activated protein kinase inhibits NF-kappaB signaling and inflammation: impact on healthspan and lifespan. *J. Mol. Med.* **89**, 667–676 (2011).
49. Canto, C. & Auwerx, J. AMP-activated protein kinase and its downstream transcriptional pathways. *Cell. Mol. Life Sci.* **67**, 3407–3423 (2010).
50. Herrero-Martin, G. et al. TAK1 activates AMPK-dependent cytoprotective autophagy in TRAIL-treated epithelial cells. *EMBO J.* **28**, 677–685 (2009).
51. Momcilovic, M., Hong, S. P. & Carlson, M. Mammalian TAK1 activates Snf1 protein kinase in yeast and phosphorylates AMP-activated protein kinase in vitro. *J. Biol. Chem.* **281**, 25336–25343 (2006).
52. Salatto, C. T. et al. Selective activation of AMPK β 1-containing isoforms improves kidney function in a rat model of diabetic nephropathy. *J. Pharmacol. Exp. Ther.* **361**, 303–311 (2017).
53. Phadtare, S., Abali, E. & Brodsky, B. Over the counter drugs (and dietary supplement) exercise: a team-based introduction to biochemistry for health professional students. *Biochem. Mol. Biol. Educ.* **41**, 384–387 (2013).
54. Zhang, J. et al. Synergistic action of 5Z-7-oxozeaenol and bortezomib in inducing apoptosis of Burkitt lymphoma cell line Daudi. *Tumour Biol.* **37**, 531–539 (2016).
55. Domcke, S., Sinha, R., Levine, D. A., Sander, C. & Schultz, N. Evaluating cell lines as tumor models by comparison of genomic profiles. *Nat. Commun.* **4**, 2126 (2013).
56. Kwok, A. L. et al. Caution over use of ES2 as a model of ovarian clear cell carcinoma. *J. Clin. Pathol.* **67**, 921–922 (2014).
57. Mi, H., Muruganujan, A. & Thomas, P. D. PANTHER in 2013: modeling the evolution of gene function, and other gene attributes, in the context of phylogenetic trees. *Nucleic Acids Res.* **41**, D377–D386 (2013).
58. Yung, M. M. et al. GRO- α and IL-8 enhance ovarian cancer metastatic potential via the CXCR2-mediated TAK1/NF κ B signaling cascade. *Theranostics* **8**, 1270–1285 (2018).
59. Listenberger, L. L. & Brown, D. A. Fluorescent detection of lipid droplets and associated proteins. *Curr. Protoc. Cell Biol.* **35**, 24-2 (2007).
60. Wei, B. R. et al. Serum S100A6 concentration predicts peritoneal tumor burden in mice with epithelial ovarian cancer and is associated with advanced stage in patients. *PLoS One* **4**, e7670 (2009).
61. Bouvet, M. et al. Real-time optical imaging of primary tumor growth and multiple metastatic events in a pancreatic cancer orthotopic model. *Cancer Res.* **62**, 1534–1540 (2002).
62. Yang, M. et al. Direct external imaging of nascent cancer, tumor progression, angiogenesis, and metastasis on internal organs in the fluorescent orthotopic model. *Proc. Natl Acad. Sci. USA* **99**, 3824–3829 (2002).
63. Chen, R. R. et al. Proteomic analysis: Compare the proteomic profiling of ES-2 and OVCA433 cells in OCM vs DMEM control. *figshare* <https://doi.org/10.6084/m9.figshare.7352000> (2019).
64. Chen, R. R. et al. Lipidomic analysis. *figshare* <https://doi.org/10.6084/m9.figshare.7351994> (2019).
65. Chen, R. R. et al. Source data: Raw data for all graphs with line or bar charts analyzed by GRAPHPAD PRISM software. *figshare* <https://doi.org/10.6084/m9.figshare.7351991> (2019).

Acknowledgements

We thank Prof. DG Hardie (School of Life Sciences, University of Dundee) provided reagents of AMPK and comments on this paper, Prof. Benjamin Tsang (Department of Obstetrics and Gynecology, University of Ottawa) for providing ovarian cancer cell lines; A2780cp SKOV3 and ES-2, Prof. George Tsao (School of Biomedical Sciences, LKS Faculty of Medicine, The University of Hong Kong) for OVCA433, and Prof. Alice Wong (School of Biological Sciences, The University of Hong Kong) for Hey8 cells. This study

was supported by National Natural Science Foundation of China (NSFC)—General Program (81472721).

Author contributions

R.C. and D.C. designed research; R.C., M.Y., Y.X., S.Z., L.L., R.L., R.S., and D.C. performed the experiments; T.L., H.Y., D.X., K.C., S.N., H.N., and D.C. contributed new reagents-analytic tools; R.C., R.S., H.N., and D.C. analyzed and interpreted data; R.C. and D.C. wrote the paper; H.N. and D.C. study supervision. All authors were involved in editing the paper and had final approval of the submitted and published versions.

Additional information

Supplementary information accompanies this paper at <https://doi.org/10.1038/s42003-019-0508-1>.

Competing interests: The authors declare no competing interests.

Reprints and permission information is available online at <http://npg.nature.com/reprintsandpermissions/>

Publisher's note: Springer Nature remains neutral with regard to jurisdictional claims in published maps and institutional affiliations.



Open Access This article is licensed under a Creative Commons Attribution 4.0 International License, which permits use, sharing, adaptation, distribution and reproduction in any medium or format, as long as you give appropriate credit to the original author(s) and the source, provide a link to the Creative Commons license, and indicate if changes were made. The images or other third party material in this article are included in the article's Creative Commons license, unless indicated otherwise in a credit line to the material. If material is not included in the article's Creative Commons license and your intended use is not permitted by statutory regulation or exceeds the permitted use, you will need to obtain permission directly from the copyright holder. To view a copy of this license, visit <http://creativecommons.org/licenses/by/4.0/>.

© The Author(s) 2019